

End-to-End Framework for Efficient Deep Learning Using Metasurfaces Optics

Carlos Mauricio Villegas Burgos,¹ Tianqi Yang,² Nick Vamivakas,¹ Yuhao Zhu,²

¹The Institute of Optics, University of Rochester

²Department of Computer Science, University of Rochester

Abstract

Deep learning using Convolutional Neural Networks (CNNs) has been shown to significantly out-performed many conventional vision algorithms. Despite efforts to increase the CNN efficiency both algorithmically and with specialized hardware, deep learning remains difficult to deploy in resource-constrained environments. In this paper, we propose an end-to-end framework to explore optically compute the CNNs in free-space, much like a computational camera. Compared to existing free-space optics-based approaches which are limited to processing single-channel (i.e., grayscale) inputs, we propose the first general approach, based on nanoscale metasurface optics, that can process RGB data directly from the natural scenes. Our system achieves up to an order of magnitude energy saving, simplifies the sensor design, all the while sacrificing little network accuracy. Our code is open-sourced at: <https://github.com/horizon-research/metasurface-dnn>

1 Introduction

Deep learning (a.k.a., deep neural networks, or DNNs) has become instrumental in a wide variety of tasks ranging from natural language processing (Mikolov et al. 2010, 2013; Sutskever, Vinyals, and Le 2014) and computer vision (Redmon et al. 2016; Bertinetto et al. 2016) to drug discovery (Chen et al. 2018a). However, despite enormous efforts both algorithmically (LeCun, Denker, and Solla 1990; Han, Mao, and Dally 2015) and with specialized hardware (Jouppi et al. 2017; Chen, Emer, and Sze 2016), deep learning remains difficult to deploy in resource-constrained systems due to the tight energy budgets and computational resources. The plateau of current digital semiconductor technology scaling further limits the efficiency improvements, and necessitates new computing paradigms that could move beyond current semiconductor technology.

Optical deep learning has recently gained attention because it has the potential to process DNNs at the speed of light with low energy consumption. A lens could execute Fourier transform “for free” (Goodman 2005). Leveraging this property, one could custom-design an optical system to execute convolution (or matrix multiplication) for free, too (Farhat et al. 1985; Psaltis, Brady, and Wagner 1988; Lu et al. 1989; Saxena and Fiesler 1995), since convolution is the spatial domain equivalence of Fourier transform. The effective convolution kernel is given by the optical system’s

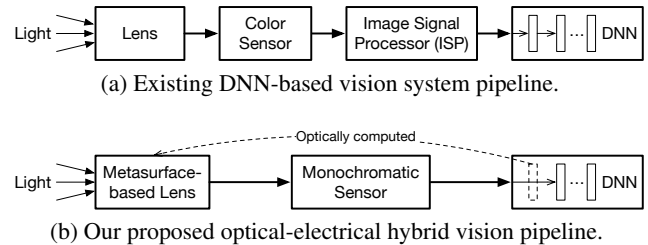


Fig. 1: Comparing our proposed system with conventional systems. Our system moves the first layer of a DNN into the optical domain based on novel metasurface-based designs. This hybrid system allows us to use a simple monochromatic sensor while completely eliminating the image signal processor (ISP), which is power-hungry and on the critical path of the traditional pipeline.

Point Spread Function (PSF), which in turn is dictated by the light *phase* change imparted by the lens.

Motivation and Challenge Existing free-space optical mechanisms can not handle layers with multiple input channels (Lin et al. 2018; Chang et al. 2018; Bueno et al. 2018), which limits the applicability to a single layer with one single input channel, e.g., MNIST hand-written digits classification. Fundamentally, this limitation is tied to their use of the Diffractive Optical Element (DOE) (O’Shea et al. 2004), which is limited to one phase profile per layer, and thus provides one single PSF (convolution kernel).

Our Solution To enable generic convolution with multiple input channels and widen the applicability of optical deep learning, we propose to use *metasurface* (Yu and Capasso 2014; Holloway et al. 2012) optics, which are ultra-thin optical elements that can produce abrupt changes on the amplitude, phase, and polarization of incident light. Due to the flexibility to shape light properties along with their ultra-compact form factor, metasurfaces are increasingly used to implement a wide range of optical functionalities.

Given a target convolution layer to be implemented optically, we purposely-design the metasurface such that each of its *meta-elements* has a unique polarization conversion efficiency (PCE) spectrum that responds to only one specific, very narrow frequency band (i.e., channel). In this way, metasurface let us apply different PSFs to different input

channels, effectively processing multi-channel inputs.

However, using metasurface optics for optical deep learning is not without challenges. Determining the metasurface parameters to produce a given PCE specification, known as the inverse design problem of metasurface, is known to be extremely time-consuming, because it involves simulating billions of design points, each of which requires solving complex Maxwell’s equations (Pestourie et al. 2018; Molesky et al. 2018). Second, an optical layer when directly plugged into a DNN model will likely not match the exact results of the mathematical convolution due to optical design imperfections and sensor artifacts (e.g., noise).

We propose an *end-to-end* optimization framework that avoids the inverse design problem altogether while minimizing the overall network loss. We start from existing metasurface designs whose PCEs are close enough to our desired PCE specifications. We then accurately model the metasurface behaviors to integrate metasurface into an end-to-end design framework, which co-optimizes the metasurface design with the rest of the network by modeling the optical layer, analog sensor, and the digital layers when executing an entire DNN model. Critically, the end-to-end pipeline is differentiable, which allows us to generate a complete system design (metasurface optical parameters and the digital layer parameters) using classic gradient descent methods.

Contributions Leveraging the end-to-end design framework, we explore a system where the first layer in a DNN is moved to the optical domain; the image sensor captures the output feature map, which is then processed in the digital domain to finish the entire network.

Our design has three advantages. First, since the sensor captures the feature map rather than the original RGB image, our system enables us to use a simple monochromatic sensor rather than a RGB sensor used in conventional systems, eliminating engineering efforts of many components such as the Color Filter Array (CFA).

Second, since we use a monochromatic sensor that captures the output feature map, we can avoid the often power-hungry computations in the image signal processor (ISP), which is required by conventional RGB sensors to correct sensor artifacts such as demosaicing and tone mapping. Avoiding ISP leads to significant overall energy reduction.

Finally, by moving the first layer into optics, we reduce the amount of computation left in the digital domain.

In summary, this paper makes the following contributions:

- We are the first to address generic (multi-channel) convolution in free-space optics. This is achieved by a novel use of metasurface optics to modulate both phase and polarization of incident light.
- We present an end-to-end differentiable optimization framework, which allows us to co-train the optical parameters and digital layer parameters to maximize the overall accuracy and efficiency.
- We evaluate our system on multiple vision networks (AlexNet, VGG, and ResNet50). Our simulation results show that our system can reduce the overall system energy by up to an order of magnitude while sacrificing an accuracy loss of 1.9% on average (0.8% minimum).

2 Related Work

Integrated Photonics DNN Existing optical deep learning systems take two major approaches: integrated photonics (Shen et al. 2017; Xia et al. 2007; Bagherian et al. 2018) and free-space photonics (Lin et al. 2018; Chang et al. 2018; Bueno et al. 2018; Hamerly et al. 2019). This paper focuses on free-space photonics. Burgos et al. (Burgos and Vamivakas 2019) propose an MLP implementation based on microring resonators (MRRs) (Bogaerts et al. 2012). Other implementations used different optical mechanisms such as Mach-Zehnder interferometers (MZI) (Shen et al. 2017; Bagherian et al. 2018), but the general principle holds. Integrated photonics circuits are fundamentally designed to execute matrix multiplications. Convolutions must be first converted to matrix multiplication, and then mapped to the photonics substrate (Bagherian et al. 2018).

The advantages of integrated photonics is that it could be directly integrated into CMOS chips, to minimize the form-factor. Integrated photonics could potentially enable optical training (Hughes et al. 2018).

The disadvantage of integrated photonics is two-fold. First, they fundamentally require coherent light (generated from a laser source) and thus could not directly operate on real-world scenes, where light is incoherent. Second, due to the quadratic propagation losses of integrated waveguides, the power consumption of the integrated photonics system could be extremely high when implementing realistic DNN models (Burgos and Vamivakas 2019). The power goes up to 500 W to execute an MLP layer with 10^5 neurons, which in turn limits the scale of the DNN to be implemented.

Free-Space Optical DNNs Motivated by the limitations of integrated photonics, recent research starts exploring free-space photonics, which exploit the physical propagation of light in the free space through custom lens to perform convolution. Chang et al. (Chang et al. 2018) is the first to demonstrate a $4-f$ system using DOEs to implement convolution layers, which support multiple output channels but does not support multiple input channels. Lin et al. (Lin et al. 2018) proposes a DOE-based free-space design, which supports a unique network architecture that is neither an MLP nor a CNN: it consists of the basic structures of an MLP, but has a limited receptive field typically found in CNNs.

Deep (Computational) Optics Implementing deep learning (convolution) in free-space optics is reminiscent of classic computational optics and computational photography, which co-designs optics with image processing and vision algorithms (Zhou and Nayar 2011). Recent progresses in deep learning has pushed this trend even further to co-train optical parameters and DNN-based vision algorithms in an end-to-end fashion. Examples include monocular depth estimation (Chang and Wetzstein 2019; Haim et al. 2018; He, Wang, and Hu 2018; Wu et al. 2019), single-short HDR imaging (Sun et al. 2020; Metzler et al. 2019), object detection (Chang and Wetzstein 2019), super-resolution and extended depth of field (Sitzmann et al. 2018).

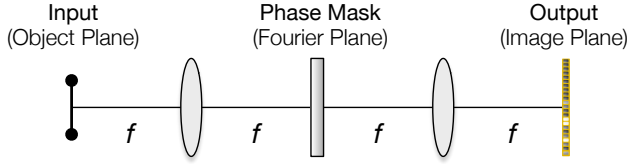


Fig. 2: A typical “4- f ” system.

3 Fundamentals of Free-Space Optics

A typical setup for free-space optical DNN is similar to computational cameras (Zhou and Nayar 2011; Ng et al. 2005), where a custom-designed lens directly interrogates the real-world scene as an optical input signal. The lens executes the first convolution or fully connected layer of a DNN; the layer output is captured by an image sensor and sent to the digital system to execute the rest of the DNN model. This setup is a natural fit for machine vision applications where the inputs are already in the optical domain and have to be captured by a camera sensor anyways.

Free space imaging scenarios can be modeled by assuming spatially incoherent light and a linear, shift-invariant optical system. Under these assumptions the image formed by an optical system (I_{out}) can be modeled as a convolution of the scene, i.e., input signal (I_{in}), with the Point Spread Function (PSF) of the optical system (Goodman 2005):

$$I_{out}(x, y, \omega) = I_{in}(x, y, \omega) \star \mathbf{PSF}(x, y) \quad (1)$$

where \star denotes convolution, $I_{in}(x, y, \omega)$ denotes the intensity of input pixel (x, y) at frequency ω , and $I_{out}(x, y, \omega)$ denotes the intensity of out pixel (x, y) at frequency ω .

Such an optical system is typically implemented using a so-called “4- f ” system (Goodman 2005) as illustrated in Fig. 2, which consists of two lenses, each with focal length f . The first lens is placed one f away from the object plane, producing a Fourier plane another f after the first lens. The second lens is placed another f from the Fourier plane, producing an inverted conjugate image plane, which is in total $4f$ from the original object plane. An image sensor is placed at the image plane to capture the output for future processing (e.g., activation and subsequent layers) in the electrical domain.

The PSF of the optical system is dictated by the *phase mask* placed at the Fourier plane. The phase mask alters the PSF by imparting certain phase change to the incident light. The phase change induced by a phase mask is called the phase mask’s *phase profile*, which is often determined by the geometric properties of the phase mask (e.g., dimension, orientation, thickness). Our goal is to find the phase profile Φ to generate a PSF that matches the target convolution kernel W . This can be formulated as an optimization problem:

$$\max_{\Phi} \|W - \mathbf{PSF}(\Phi)\|. \quad (2)$$

Without the phase mask, the image captured by the image sensor simply reproduces the input I_{in} . With the optimized phase mask, the output image is naturally the result of the convolution in Equation 1.

The optical convolution in Equation 1 can be seen as a simplification of a generic convolution layer:

$$I_{out}^j(x, y) = \sum_{i=1}^{C_{in}} I_{in}^i(x, y) \star W_{j,i}(x, y), \quad \forall j \in [1, C_{out}], \quad (3)$$

where the input channel (C_{in}) and the output channel (C_{out}) of the optical convolution are both 1. Supporting multiple output channels (i.e., multiple convolution kernels) is achieved by spatially tiling C_{out} phase masks on the same plane; each phase mask corresponds to a convolution kernel W_j . (Chang et al. 2018). As the incident light goes through the tiled phase mask, it is naturally convolved with the different PSFs (convolution kernels), effectively generating multiple output channels.

However, supporting multiple input channels is a fundamental challenge unaddressed in prior work. Essentially, the optical system must provide multiple PSFs, each of which applies to *only a particular frequency* (i.e., channel) of the incident light. This can not be achieved by simply tiling different phase masks on the same plane, which would naturally apply each PSF to *all* the frequencies in the incident light. This is an inherent limitation of prior efforts that use diffractive optical elements (DOE) (O’Shea et al. 2004) to implement the phase mask. To overcome this limitation, we instead propose to implement the phase mask using metasurfaces, which we describe in detail next.

4 Metasurface-based Optical Convolution

The goal is to design the phase mask in a way that different PSFs are applied to different input channels. Unlike DOEs that modulate only the phase of the incident light, metasurfaces are able to modulate both the phase and *polarization* of the incident light. Our key idea is to modulate the polarization such that we could control which PSF is applied to which input channel. Meanwhile, we modulate the phase in order to implement any target PSF. We first describe the phase modulation assuming only one input channel, followed by polarization modulation, which allows us to generalize free-space optical convolution to multiple channels.

4.1 Phase Modulation

Metasurface phase mask consists of a set of meta-elements, each of which induces a particular phase change to the incident light. Physically, we use the Pancharatnam-Berry (P-B) phase (Yu and Capasso 2014; Balthasar Mueller et al. 2017). P-B phase comes from the spin rotation effect that arises from the interaction between circularly-polarized light and an anisotropic meta-element (met 2017). Specifically, a meta-element that is geometrically symmetric with respect to its main axes and that has an in-plane orientation angle θ induces a geometric phase 2θ on the incident light (Chen et al. 2018b; met 2017). Therefore, for a phase mask that consists of $M \times N$ meta-elements, each having an in-plane rotation of $\theta_{m,n}$, the phase profile Φ of the phase mask is also a $M \times N$ matrix, where each element is $2 \times \theta_{m,n}$.

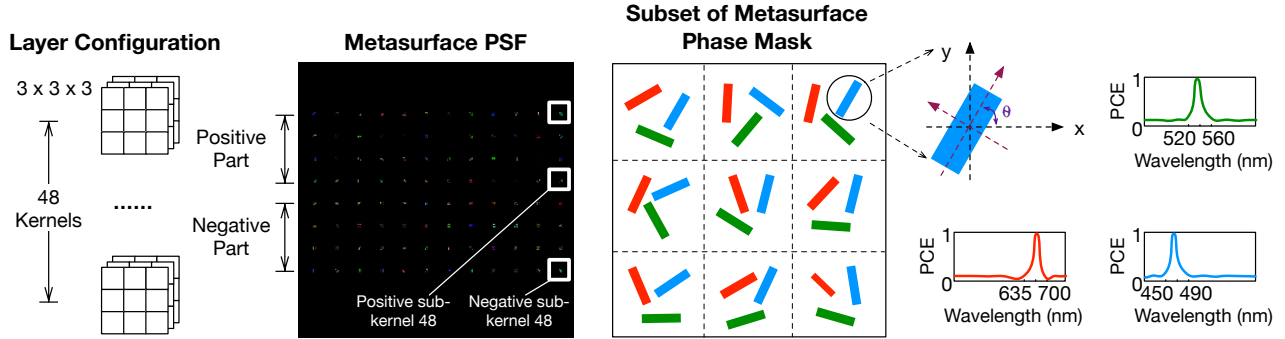


Fig. 3: A metasurface phase mask for a layer that has 48 kernels, where each kernel has 3 channels and each channel has 3×3 elements. The phase mask is arranged as 12×8 cells with 1 positive and 1 negative cell for each kernel. Each cell has 3×3 tiles. Each tile has 3 meta-elements, corresponding to the 3 channels. Each meta-element has a unique in-plane rotation θ . Within each cell, all 9 meta-elements of the same channel collectively provide a PSF that matches the corresponding channel in a convolution kernel. Meta-elements in the same channel have the same PCE spectrum, which is designed such that, in the ideal case, the corresponding PSF is applied to one particular input channel only.

In a $4-f$ system (DOE or metasurface), the PSF relates to the phase profile (Φ) of the phase mask according to the following equation:

$$\mathbf{PSF}(\Phi) = |\mathcal{F}^{-1} \{e^{i\Phi}\}|^2, \quad (4)$$

where \mathcal{F}^{-1} denotes the inverse 2D Discrete Fourier transform. Thus, finding the optimal phase profile is formulated as the following optimization problem:

$$\min_{\Phi_k} \|W_k - |\mathcal{F}^{-1} \{e^{i\Phi_k}\}|^2\|_F^2, \quad (5)$$

where $\|\cdot\|_F$ denotes the Frobenius norm, W_k denotes the k^{th} channel of the target convolution kernel, Φ_k denotes the discretized 2D phase profile of channel k , and has the same dimension as W_k .

With the optimized Φ_k , we simply divide each of its elements by 2 to obtain the orientation of each meta-element. Note the objective function is differentiable (Goodman 2005). Thus, phases could be co-optimized with the rest of DNN in an end-to-end fashion, as we will show in Sec. 5.

Since PSF physically corresponds to light intensity (Goodman 2005) and there is no negative light intensity, the negative values in a kernel cannot be physically implemented. A mathematical explanation is that the PSF is the square form of an expression, as shown in Equation 4, and thus must be non-negative. To address this limitation, we use the idea of Chang et. al. (Chang et al. 2018) by splitting a kernel into two *sub-kernels*; one contains only the positive portion and the other contains only the negative portion of the kernel. The final kernel is calculated by subtracting the negative sub-kernel from the positive sub-kernel.

As a result, for a layer that has K kernels, there are $2K$ phase profiles to be individually optimized. In reality, we could tile the $2K$ sub-kernels in one plane and optimize the $2K$ phase profiles together. Fig. 3 shows the phase mask for a layer that has 48 kernels, each of dimension $3 \times 3 \times 3$. The phase mask has 96 cells, where the top half is the phase masks for the positive sub-kernels and the bottom half is

phase masks for the negative sub-kernels. Each cell consists of 3×3 tiles, corresponding to the 3×3 elements in a channel. The in-plane rotation of each meta-element is optimized from Equation 5. The three meta-elements in a cell correspond to the three channels, which we discuss next.

4.2 Polarization Modulation

Now we are able to engineer the PSF to match any given 2D matrix (i.e., a channel in the target kernel), the remaining challenge is that the same PSF of a meta-element would be imposed on all three channels in the input light, whereas to correctly implement a convolution layer we must make sure each PSF applies to only one particular input channel.

We exploit the fact that each meta-element acts as a phase retarder, imposing a polarization conversion efficiency (PCE) on each wavelength. Effectively, the corresponding intensity of output pixel (x, y) at frequency ω is weighted by $\text{PCE}(\omega)$. With PCE, the contribution of an input channel c to an output channel is:

$$I_{con}^c(x, y, \omega) = \sum_{c'=1}^{C_{in}} \text{PCE}^{c'}(\omega) (\mathbf{PSF}^{c'}(\eta, \xi) \star I_{in}^c(\eta, \xi, \omega)), \quad (6)$$

where channel c of the input image is affected by the PSF of every channel c' in metasurface, which is where the sum over PSF channels c' comes from.

In the ideal case, the PCE is a delta function that is 1 for a very narrow band, e.g., red wavelength, and 0 for all other wavelengths. That way, the PSF carried by the meta-elements will effectively convolve only with a particular input channel. Fig. 3 shows an example that support 3 input channels (e.g., natural light from the real-world). The key is that each cell consists of three meta-elements, each carrying a unique PCE. When white light containing the RGB wavelengths (channels) is incident on the phase mask, the red channel will acquire the phase imparted by the red meta-element only, mimicking the convolution between the red

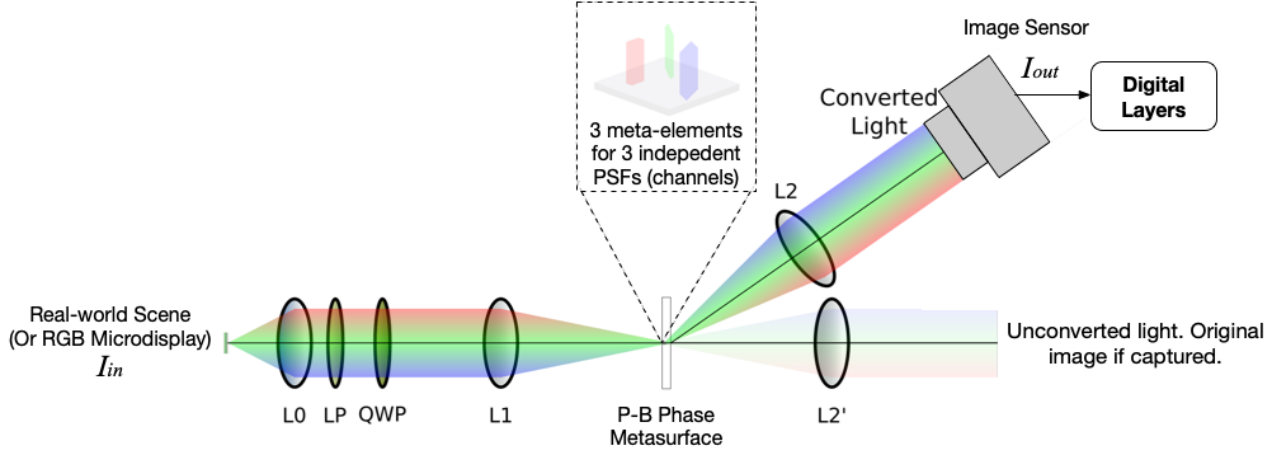


Fig. 4: Hardware system. Light from the real-world (or a microdisplay) is collimated by lens L0, and then goes through a linear polarizer (LP) and a broadband quarter-wave plate (QWP) so that light becomes circularly-polarized. The plane of the LP is the input plane of the $4f$ system. A metasurface phase mask is placed at the Fourier plane. A portion of the light gets the engineered phase shift and has its polarization handedness switched. This “converted” portion of the light gets sent to lens L2, via a phase “grating” (Palmer and Loewen 2002) to the phase mask, while the unconverted light is sent to lens L2’ on the optical axis. L2 is at a distance f from the metasurface. Finally, light is detected by the image sensor placed at a distance f after L2.

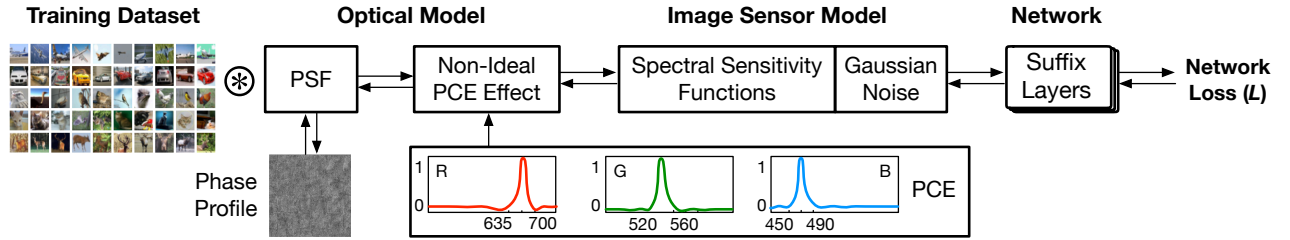


Fig. 5: End-to-end training framework. The polarization profile is network-independent, and is obtained from real metasurface optics fabrications. The phase profile is network-dependent; it is trained using the training data, and fine-tuned with the DNN model suffix layers (i.e., layers implemented in the digital domain) together in an end-to-end fashion.

channel and the corresponding PSF; the same process applies to green and blue wavelengths as well. The output is naturally the superposition (sum of intensity) of the three convolution outputs.

In reality, the metasurface design is regulated by fabrication constraints and, thus, the actual PCE will never be an ideal delta function, which leads to cross-talk, i.e., the PSF of a channel i will be convolved with input channel j . Therefore, it is critical to optimize the end-to-end system to minimize the impact of cross-talk, which we discuss next.

5 End-to-End Training Framework

Fig. 4 shows the end-to-end system setup, from light in the real-world scene (or equivalently a RGB microdisplay) to the network output. It consists primarily of three components: a metasurface-based optical system that implements the first convolution layer of a DNN, an image sensor that captures the output of the optical convolution, and a digital processor that finishes the rest of the network, which we call the “suffix layers.”

In order to maximize the overall network accuracy, we co-optimize the optical convolution layer with digital layers in an end-to-end fashion. Fig. 5 shows the end-to-end differentiable pipeline, which incorporates three components: an optical model, a sensor model, and the digital network. The phase profile (Φ) in the optical model and the suffix layer weights (W) are optimization variables. The loss function is the same as that of the original network.

The input to the system is light, which in practical applications are from the real-world scene. In our experiments, we use a RGB microdisplay displaying images from datasets to emulate the real-world scene as is done in prior work (Chang et al. 2018). Thus, channel c in the input is expressed as:

$$I_{in}^c(x, y, \omega) = \text{SPD}^c(\omega) I_{in}^c(x, y), \quad (7)$$

where $\text{SPD}^c(\omega)$ is the spectral power distribution of color channel c in the input light at frequency ω , and $I_{in}^c(x, y)$ is the light intensity of pixel (x, y) in channel c and is directly read from the RGB image in the training data.

In the forward pass during training (and also inference),

the PSF generated from the phase profile (Φ) is first convolved with the input image from a training dataset under the impact of the PCE as described by Equation 6. The convolution output is captured by the image sensor, which we model by its spectral sensitivity function (SSF). In addition, image sensors introduce different forms of noise, which we model as a Gaussian noise $N(\mu, \sigma^2)$ based on the central limit theorem. As a result, a channel in the output image captured by the sensor is given by:

$$I_{out}(x, y) = \sum_{c=1}^{C_{in}} \int \mathbf{SSF}(\omega) I_{con}^c(x, y, \omega) d\omega + N(\mu, \sigma^2). \quad (8)$$

Note that the sum across different input channels, required by correctly implementing a convolution layer, is realized in our design “for free” by superimposing the outputs of different phase masks. The light intensity of the superimposed output is naturally the sum of the intensities of individual channel outputs.

Plugging Equation 7 into Equation 6 and plugging Equation 6 into Equation 8 yields the sensor output, which becomes the input to the digital suffix layers to produce the network loss. Note that the convolution layer mapped to metasurface, as described by Equation 8, is differentiable, and thus enables end-to-end training using classic gradient descent-based optimization methods.

During back-propagation, the phase profile (Φ) and the digital layer weights (W) are optimized. Note that the PCEs of the meta-elements are network-independent, and are directly obtained from fabrication. They are kept fixed throughout training.

Practical Considerations Since different sub-kernels are tiled together for the ease of training, the outputs of different sub-convolutions (i.e., convolution between a sub-kernel and the corresponding channel in the input) will be tiled too. We must make sure that the different sub-convolution outputs do not overlap so that we can assemble them (digitally) to form the actual convolution output.

To that end, we pad each sub-kernel with space between cells in the phase mask. For instance in Fig. 3, we pad each 3×3 sub-kernel by 8 pixels each side to form a 19×19 matrix, effectively separating neighboring cells in the phase mask by 16 pixels. As a result, the outputs of each sub-kernel will be separated by that much, too. In summary, given the kernels in a target convolution layer, we first separate each kernel into two sub-kernels, tile all the sub-kernels together, and then add padding to form the actual target weight matrix, for which we then apply the phase optimization described in Equation 5 to derive the rotation of each meta-element.

Monochromatic Sensor It is important to note that our system design let us use a simple monochromatic sensor rather than a conventional RGB sensor. This is because of two reasons. First, the results of all output channels lie completely within a 2D plane, because the phase masks of different convolution kernels and of different channels within a kernel are tiled in a 2D plane (Fig. 3). Second, the result of each output channel is naturally “calculated” by superimposing the output lights of each individual input channels.

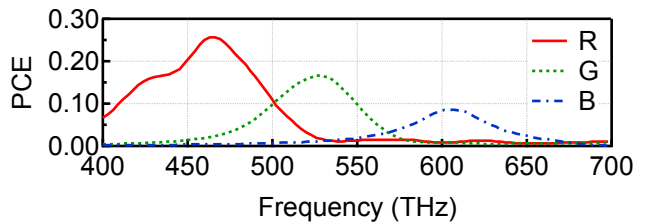


Fig. 6: PCEs of the three metasurface designs.

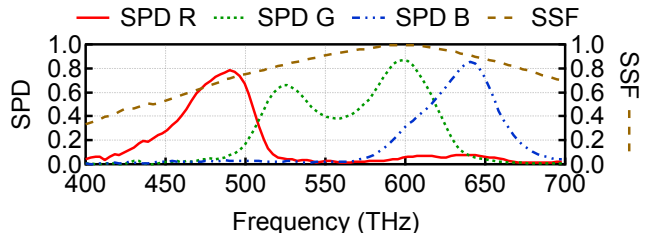


Fig. 7: The spectral power distributions (SPDs) of the microdisplay and the spectral sensitivity function (SSF) of the image sensor modeled in our experiments.

6 Evaluation

6.1 Methodology

Networks and Datasets We implement the end-to-end training framework in TensorFlow. We differentiate the metasurface optics layer (from phase profile to the target kernel) and integrate the differentiation into the back-propagation process.

We evaluate on three networks: AlexNet (Krizhevsky, Sutskever, and Hinton 2012), VGG-16 (Simonyan and Zisserman 2014), and ResNet50 (Szegedy et al. 2017), all on the CIFAR-100 dataset (Krizhevsky, Hinton et al. 2009).

Training Details To accelerate convergence, we first train the entire network in three separate steps: 1) train the entire network digitally, 2) use the first layer’s weights to optimize the phase mask, and 3) finally the optimized phase mask and the pre-trained suffix layers are and then fine-tuned end-to-end until convergence.

The phase optimization is all networks is optimized using gradient descent and the results converge after 2,000 iterations. The phase masks are then end-to-end fine-tuned with the suffix layers for 50, 150, and 50 epochs for AlexNet, VGG, and ResNet, respectively.

Hardware Modeling Details The metasurface designs we use are from Wang et al. (Wang et al. 2016), which provide the detailed design specifications of three kinds of meta-elements, each of which is designed to generate the highest response at red, green, and blue band of the spectrum. From the design specifications, we run the well-known MEEP package (Oskooi et al. 2010, 2020) for electromagnetics simulations to generate the corresponding PCEs of the three metasurfaces, which we use in our design and simulation. Fig. 6 shows the PCE of the three metasurfaces. While the PCEs are not ideal delta functions, they do provide the highest responses in distinct bands.

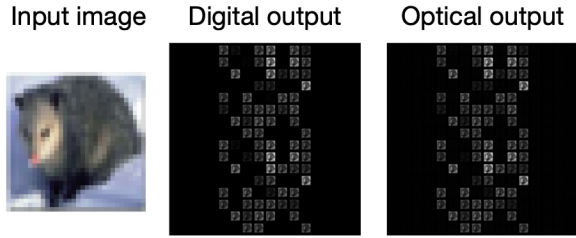
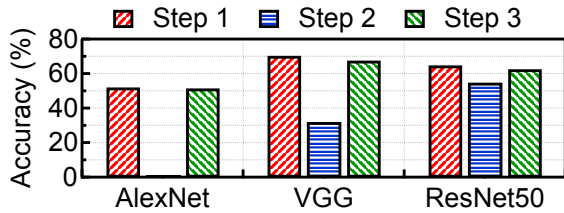
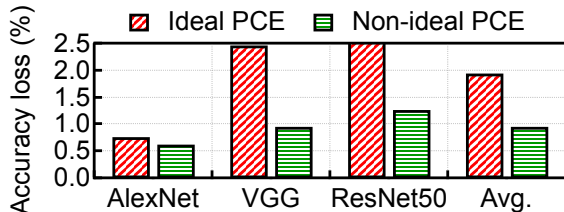


Fig. 8: Comparison between first layer output implemented digitally and implemented optically.



(a) Accuracy comparison using actual metasurface designs.



(b) Comparing accuracy loss of Step 3 (our design) from Step 1 (fully digital) between using ideal and non-ideal PCEs.

Fig. 9: Accuracy results.

We use the Sony ICX274AL image sensor, whose SSF we adapt from the design specification (Sony 2020). We use the eMagin OLED-XL RGB microdisplay from eMagin, whose SPDs we obtained by contacting the display manufacturer. Fig. 7 shows the SPDs of the microdisplay (left y -axis) and the SSF of the sensor (right y -axis). Comparing the SPDs and the PCEs in Fig. 6, the PCE and SPD peaks match (e.g., both the red PCE and the red light from the microdisplay peak at around 450 THz to 500 THz), suggesting that the cross-talk across channels is small.

6.2 Network Accuracy and Efficiency

Phase Optimization We find that our phase optimization allows us to generate a PSF that resembles the target kernel. The loss approaches 10^{-4} after 2,000 iterations. Fig. 8 compares the output feature map of the first layer between the digital implementation and the optical implementation, which match well, indicating that the optical output provides a desirable input to the suffix digital layers. Note that the different output channels are tiled in one 2D plane.

Accuracy We find that our end-to-end design leads to little accuracy loss. Fig. 9a shows the network accuracies of the three training steps. As we can see, step 1 is the origi-

nal network executed fully in the digital domain, and generally has the highest accuracy. Step 2 optimizes the PSF from the target convolution kernel and directly integrates the optimized PSF into the network; this leads to significant lower accuracy. However, after end-to-end fine-tuning with the suffix layers, we could largely gain the accuracy loss. Overall across the three networks, our optical-electrical DNN system leads to on average only an 1.9% (0.8% minimum) accuracy loss compared to fully-digital networks.

The accuracy loss could be further improved if we could improve the PCE of the metasurface designs. Fig. 9b compares the accuracy loss on the three networks between using ideal PCEs (i.e., delta functions) and non-ideal PCEs (from actual designs, used in Fig. 9a). Using an ideal PCE leads to an average accuracy loss of only 0.9%. This suggests that our system design can readily benefit from better metasurface designs in the future.

Efficiency Our system reduces the overall compute cost in two ways. First, we completely avoid the need to process raw sensor data using the power-hungry ISP. Traditional vision systems use ISP to process raw sensor data (e.g., demosaic, tone mapping) to generate RGB images for the DNN to process, but since in our system the image sensor captures the output feature map rather than the RGB image, the ISP processing could be avoided.

We measure the power of the Nvidia’s Jetson TX2 board, which is representative of today’s high-end systems for mobile vision (Nvidia 2018). The ISP consumes about 0.5 mJ of energy to generate one RGB frame. In contrast, the energy consumed to process AlexNet, VGG, and ResNet50 is 0.31 mJ, 0.36 mJ, 0.05 mJ, respectively. Avoiding the ISP yields $2.4\times$ to one order of magnitude energy saving.

Secondarily, by pushing the first CNN layer into the optical domain, we also reduce the total amount of computations (measured in the number of multiply-accumulate, or MAC, operations) to compute the DNN. In AlexNet, the MAC saving is 4.4%, and the MAC saving is 0.8% and 0.5% for ResNet50 and VGG, respectively.

7 Discussion and Conclusion

This paper demonstrates the first free-space optics approach that enables general convolution. The significance our system is three-fold. First, it eliminates the need for the power-hungry ISP. Second, it simplifies the sensor design and enables the use of a simple monochromatic sensor rather than a RGB sensor. Finally, it reduces the computation to execute a DNN. Overall, we show an order of magnitude of energy saving with 1.9% on average (0.8% minimum) accuracy.

We are in the process of fabricating an optical prototype. While our current design pushes only the first DNN layer into optics, pushing more layers into optics is possible but not without challenges. The key challenge is that it is difficult to optically implement non-linear functions, which usually have to be implemented in the electrical domain, introducing optical-electrical interface transduction overhead. Therefore, a future direction is to comprehensively explore the hybrid optical-electrical design space to evaluate the optimal partition between optics and electronics.

References

2017. Metasurface optical holography. *Materials Today Physics* 3: 16 – 32. ISSN 2542-5293. doi:<https://doi.org/10.1016/j.mtphys.2017.11.001>.
- Bagherian, H.; Skirlo, S.; Shen, Y.; Meng, H.; Ceperic, V.; and Soljacic, M. 2018. On-Chip Optical Convolutional Neural Networks. *arXiv preprint arXiv:1808.03303*.
- Balthasar Mueller, J. P.; Rubin, N. A.; Devlin, R. C.; Groever, B.; and Capasso, F. 2017. Metasurface Polarization Optics: Independent Phase Control of Arbitrary Orthogonal States of Polarization. *Phys. Rev. Lett.* 118: 113901. doi:10.1103/PhysRevLett.118.113901. URL <https://link.aps.org/doi/10.1103/PhysRevLett.118.113901>.
- Bertinetto, L.; Valmadre, J.; Henriques, J. F.; Vedaldi, A.; and Torr, P. H. 2016. Fully-convolutional siamese networks for object tracking. In *European conference on computer vision*, 850–865. Springer.
- Bogaerts, W.; De Heyn, P.; Van Vaerenbergh, T.; De Vos, K.; Kumar Selvaraja, S.; Claes, T.; Dumon, P.; Bienstman, P.; Van Thourhout, D.; and Baets, R. 2012. Silicon microring resonators. *Laser & Photonics Reviews* 6(1): 47–73.
- Bueno, J.; Maktoobi, S.; Froehly, L.; Fischer, I.; Jacquot, M.; Larger, L.; and Brunner, D. 2018. Reinforcement learning in a large-scale photonic recurrent neural network. *Optica* 5(6): 756–760.
- Burgos, C. M. V.; and Vamivakas, N. 2019. Challenges in the Path Toward a Scalable Silicon Photonics Implementation of Deep Neural Networks. *IEEE Journal of Quantum Electronics* 55(5): 1–10.
- Chang, J.; Sitzmann, V.; Dun, X.; Heidrich, W.; and Wetzstein, G. 2018. Hybrid optical-electronic convolutional neural networks with optimized diffractive optics for image classification. *Scientific reports* 8(1): 12324.
- Chang, J.; and Wetzstein, G. 2019. Deep optics for monocular depth estimation and 3d object detection. In *Proceedings of the IEEE International Conference on Computer Vision*, 10193–10202.
- Chen, H.; Engkvist, O.; Wang, Y.; Olivecrona, M.; and Blaschke, T. 2018a. The rise of deep learning in drug discovery. *Drug discovery today* 23(6): 1241–1250.
- Chen, W. T.; Zhu, A. Y.; Sanjeev, V.; Khorasaninejad, M.; Shi, Z.; Lee, E.; and Capasso, F. 2018b. A broadband achromatic metalens for focusing and imaging in the visible. *Nature Nanotechnology* 13(3): 220–226. doi:10.1038/s41565-017-0034-6. URL <https://doi.org/10.1038/s41565-017-0034-6>.
- Chen, Y.-H.; Emer, J.; and Sze, V. 2016. Eyeriss: A spatial architecture for energy-efficient dataflow for convolutional neural networks. In *ACM SIGARCH Computer Architecture News*, volume 44, 367–379. IEEE Press.
- Farhat, N. H.; Psaltis, D.; Prata, A.; and Paek, E. 1985. Optical implementation of the Hopfield model. *Applied optics* 24(10): 1469–1475.
- Goodman, J. W. 2005. *Introduction to Fourier optics*. Roberts and Company Publishers.
- Haim, H.; Elmalem, S.; Giryas, R.; Bronstein, A. M.; and Marom, E. 2018. Depth estimation from a single image using deep learned phase coded mask. *IEEE Transactions on Computational Imaging* 4(3): 298–310.
- Hamerly, R.; Bernstein, L.; Sludds, A.; Soljačić, M.; and Englund, D. 2019. Large-scale optical neural networks based on photoelectric multiplication. *Physical Review X* 9(2): 021032.
- Han, S.; Mao, H.; and Dally, W. J. 2015. Deep compression: Compressing deep neural networks with pruning, trained quantization and Huffman coding. *arXiv preprint arXiv:1510.00149*.
- He, L.; Wang, G.; and Hu, Z. 2018. Learning depth from single images with deep neural network embedding focal length. *IEEE Transactions on Image Processing* 27(9): 4676–4689.
- Holloway, C. L.; Kuester, E. F.; Gordon, J. A.; O’Hara, J.; Booth, J.; and Smith, D. R. 2012. An Overview of the Theory and Applications of Metasurfaces: The Two-Dimensional Equivalents of Metamaterials. *IEEE Antennas and Propagation Magazine* 54(2): 10–35. ISSN 1045-9243. doi:10.1109/MAP.2012.6230714.
- Hughes, T. W.; Minkov, M.; Shi, Y.; and Fan, S. 2018. Training of photonic neural networks through in situ backpropagation and gradient measurement. *Optica* 5(7): 864–871.
- Jouppi, N. P.; Young, C.; Patil, N.; Patterson, D.; Agrawal, G.; Bajwa, R.; Bates, S.; Bhatia, S.; Boden, N.; Borchers, A.; et al. 2017. In-datacenter performance analysis of a tensor processing unit. In *2017 ACM/IEEE 44th Annual International Symposium on Computer Architecture (ISCA)*, 1–12. IEEE.
- Krizhevsky, A.; Hinton, G.; et al. 2009. Learning multiple layers of features from tiny images. Technical report, Cite-seer.
- Krizhevsky, A.; Sutskever, I.; and Hinton, G. E. 2012. Imagenet classification with deep convolutional neural networks. In *Advances in neural information processing systems*, 1097–1105.
- LeCun, Y.; Denker, J. S.; and Solla, S. A. 1990. Optimal brain damage. In *Advances in neural information processing systems*, 598–605.
- Lin, X.; Rivenson, Y.; Yardimci, N. T.; Veli, M.; Luo, Y.; Jarrahi, M.; and Ozcan, A. 2018. All-optical machine learning using diffractive deep neural networks. *Science* 361(6406): 1004–1008.
- Lu, T.; Wu, S.; Xu, X.; and Francis, T. 1989. Two-dimensional programmable optical neural network. *Applied optics* 28(22): 4908–4913.
- Metzler, C. A.; Ikoma, H.; Peng, Y.; and Wetzstein, G. 2019. Deep Optics for Single-shot High-dynamic-range Imaging. *arXiv preprint arXiv:1908.00620*.
- Mikolov, T.; Karafiát, M.; Burget, L.; Černocký, J.; and Khudanpur, S. 2010. Recurrent neural network based language model. In *Eleventh annual conference of the international speech communication association*.

- Mikolov, T.; Sutskever, I.; Chen, K.; Corrado, G. S.; and Dean, J. 2013. Distributed representations of words and phrases and their compositionality. In *Advances in neural information processing systems*, 3111–3119.
- Molesky, S.; Lin, Z.; Piggott, A. Y.; Jin, W.; Vucković, J.; and Rodriguez, A. W. 2018. Inverse design in nanophotonics. *Nature Photonics* 12(11): 659–670.
- Ng, R.; Levoy, M.; Brédif, M.; Duval, G.; Horowitz, M.; Hanrahan, P.; et al. 2005. Light field photography with a hand-held plenoptic camera. *Computer Science Technical Report CSTR 2(11)*: 1–11.
- Nvidia. 2018. NVIDIA Jetson TX2 Delivers Twice the Intelligence to the Edge. URL <https://devblogs.nvidia.com/jetson-tx2-delivers-twice-intelligence-edge/>.
- O’Shea, D. C.; Suleski, T. J.; Kathman, A. D.; and Prather, D. W. 2004. *Diffraction optics: design, fabrication, and test*, volume 62. Spie Press Bellingham, WA.
- Oskooi, A. F.; Roundy, D.; Ibanescu, M.; Bermel, P.; Joannopoulos, J. D.; and Johnson, S. G. 2010. MEEP: A flexible free-software package for electromagnetic simulations by the FDTD method. *Computer Physics Communications* 181(3): 687–702.
- Oskooi, A. F.; Roundy, D.; Ibanescu, M.; Bermel, P.; Joannopoulos, J. D.; and Johnson, S. G. 2020. Meep: free finite-difference time-domain (FDTD) software for electromagnetic simulations. <https://github.com/NanoComp/meep>.
- Palmer, C. A.; and Loewen, E. G. 2002. *Diffraction grating handbook*, volume 5. Thermo RGL New York.
- Pestourie, R.; Pérez-Arancibia, C.; Lin, Z.; Shin, W.; Capasso, F.; and Johnson, S. G. 2018. Inverse design of large-area metasurfaces. *Optics express* 26(26): 33732–33747.
- Psaltis, D.; Brady, D.; and Wagner, K. 1988. Adaptive optical networks using photorefractive crystals. *Applied Optics* 27(9): 1752–1759.
- Redmon, J.; Divvala, S.; Girshick, R.; and Farhadi, A. 2016. You only look once: Unified, real-time object detection. In *Proceedings of the IEEE conference on computer vision and pattern recognition*, 779–788.
- Saxena, I.; and Fiesler, E. 1995. Adaptive multilayer optical neural network with optical thresholding. *Optical Engineering* 34(8): 2435–2440.
- Shen, Y.; Harris, N. C.; Skirlo, S.; Prabhu, M.; Baehr-Jones, T.; Hochberg, M.; Sun, X.; Zhao, S.; Larochelle, H.; Englund, D.; et al. 2017. Deep learning with coherent nanophotonic circuits. *Nature Photonics* 11(7): 441.
- Simonyan, K.; and Zisserman, A. 2014. Very deep convolutional networks for large-scale image recognition. *arXiv preprint arXiv:1409.1556*.
- Sitzmann, V.; Diamond, S.; Peng, Y.; Dun, X.; Boyd, S.; Heidrich, W.; Heide, F.; and Wetzstein, G. 2018. End-to-end optimization of optics and image processing for achromatic extended depth of field and super-resolution imaging. *ACM Transactions on Graphics (TOG)* 37(4): 1–13.
- Sony. 2020. ICX274AL sensor specification. https://www.lstvision.com/cameras/sensor_specs/ICX274.pdf.
- Sun, Q.; Tseng, E.; Fu, Q.; Heidrich, W.; and Heide, F. 2020. Learning Rank-1 Diffractive Optics for Single-shot High Dynamic Range Imaging. In *Proceedings of the IEEE Conference on Computer Vision and Pattern Recognition*.
- Sutskever, I.; Vinyals, O.; and Le, Q. V. 2014. Sequence to sequence learning with neural networks. In *Advances in neural information processing systems*, 3104–3112.
- Szegedy, C.; Ioffe, S.; Vanhoucke, V.; and Alemi, A. A. 2017. Inception-v4, inception-resnet and the impact of residual connections on learning. In *Thirty-First AAAI Conference on Artificial Intelligence*.
- Wang, B.; Dong, F.; Li, Q.-T.; Yang, D.; Sun, C.; Chen, J.; Song, Z.; Xu, L.; Chu, W.; Xiao, Y.-F.; et al. 2016. Visible-frequency dielectric metasurfaces for multiwavelength achromatic and highly dispersive holograms. *Nano letters* 16(8): 5235–5240.
- Wu, Y.; Boominathan, V.; Chen, H.; Sankaranarayanan, A.; and Veeraraghavan, A. 2019. PhaseCam3D—Learning Phase Masks for Passive Single View Depth Estimation. In *2019 IEEE International Conference on Computational Photography (ICCP)*, 1–12. IEEE.
- Xia, F.; Rooks, M.; Sekaric, L.; and Vlasov, Y. 2007. Ultra-compact high order ring resonator filters using submicron silicon photonic wires for on-chip optical interconnects. *Optics express* 15(19): 11934–11941.
- Yu, N.; and Capasso, F. 2014. Flat optics with designer metasurfaces. *Nature Materials* 13(2): 139–150. doi: 10.1038/nmat3839. URL <https://doi.org/10.1038/nmat3839>.
- Zhou, C.; and Nayar, S. K. 2011. Computational cameras: convergence of optics and processing. *IEEE Transactions on Image Processing* 20(12): 3322–3340.